Physics of Fluids

Variational approach to dynamic contact angles for thin films

Cite as: Phys. Fluids **30**, 082115 (2018); https://doi.org/10.1063/1.5040985
Submitted: 22 May 2018 . Accepted: 09 August 2018 . Published Online: 29 August 2018

Dirk Peschka

Variational approach to dynamic contact angles for thin films

Dirk Peschka[a)]
Weierstrass Institute for Applied Analysis and Stochastics, Berlin, Germany

(Received 22 May 2018; accepted 9 August 2018; published online 29 August 2018)

This paper investigates a modeling approach for viscous flows with dynamic contact angles based on variational energy-dissipation principles. A corresponding Stokes free boundary problem is reduced to a thin-film equation and its variational structure is constructed. The usefulness of this abstract modeling approach is demonstrated by providing numerical schemes for the Stokes flow and the thin-film model and by computing numerical solutions for the problem of gravity-driven thin droplets. Some implications of the contact angle model and properties of the numerical scheme are highlighted in this setting. *Published by AIP Publishing.* https://doi.org/10.1063/1.5040985

I. INTRODUCTION

The wetting and dewetting flow of a thin layer of a viscous liquid over a solid planar surface has supplied researchers with a valuable model system to study a number of interesting fluid problems.[1–3] Related phenomena appear in nature but are also of great importance for applications, e.g., droplet splashing, wetting, coating, painting, pattern formation processes, multiphase flows, and microfluidics, to name only a few. The mathematical and numerical analysis of the corresponding free boundary problems is considered quite challenging.

The contact line is where solid, liquid, and air phase meet. In equilibrium, interfacial tensions between solid-air $\sigma_{\text{solid,air}}$, solid-liquid $\sigma_{\text{solid,liquid}}$, and liquid-air $\sigma_{\text{liquid,air}} \equiv \sigma_\ell$ lead to a contact angle $\vartheta = \vartheta_e$ that is determined by the famous Young-Dupré equation

$$\sigma_\ell(\cos(\vartheta_e) - 1) = S, \tag{1}$$

where the spreading coefficient of the system is defined as $S = \sigma_{\text{solid,air}} - (\sigma_{\text{solid,liquid}} + \sigma_{\text{liquid,air}})$ and is assumed to be negative. For soft surfaces, this condition is replaced by the Neumann triangle construction.

A discussion about *contact line dynamics* starts with the boundary condition at the solid-liquid interface. Sliding contact lines with a no-slip condition create a logarithmic singularity in the energy dissipation, and different regularization mechanisms for this have been proposed, e.g., using a Navier-slip condition.[4,5] The corresponding regularization parameter *slip-length* has a physical interpretation and its existence is confirmed experimentally,[6] and thin-film models with different magnitudes of slip-lengths have been investigated.[7] The discussion becomes much more involved for contact lines moving over physically realistic nonideal surfaces, e.g., which are not perfectly smooth, rigid, or chemically homogeneous. Then, in the Young-Dupré equation (1), the spreading coefficient needs to be replaced with a homogenized coefficient $\bar{S}$ using the Cassie-Baxter relation.[8] However, the corresponding equilibrium angle might never be attained, since, due to pinning at microscopic defects, the contact line is stationary for contact angles $\vartheta_r < \vartheta < \vartheta_a$ and only advances or recedes beyond these values; see Fig. 1.

There is a rich literature showing different approaches for contact angle models[9–13] including variational or heuristic approaches for sliding or rolling motion. Models for smooth contact angle dynamics without hysteresis are often based on empirical laws and on microscopic theories. For instance, assuming an energy-dissipation balance truncated at a microscopic length scale L_{micro} and with a macroscopic length scale L_{macro} away from the contact line, the theory by Cox[14] and Voinov[15] predicts

$$\vartheta^3 - \vartheta_e^3 = \pm 9\,\text{Ca}\,\ln(L_{\text{macro}}/L_{\text{micro}}),$$

where the capillary number $\text{Ca} = \mu U/\sigma_\ell$ depends on dynamic viscosity μ, liquid-air surface tension σ_ℓ, and contact line velocity U. Most models considered in the literature are of the form $R(\vartheta, \vartheta_e) = \pm\text{Ca}$, where usually R is a polynomial with $R(\vartheta_e, \vartheta_e) = 0$. In molecular-kinetic theory, the dynamic contact angle is determined by the random motion of molecules near the contact line. This theory also allows to deduce a theory of wetting,[12,16,17] where the contact line velocity can be expressed as $U \sim \sinh\left[\lambda^2\sigma_\ell(\cos\vartheta_e - \cos\vartheta)/(2k_BT)\right]$ and λ encodes an average molecular displacement. On the continuum level, nonequilibrium variational approaches found[11,12] linearized variants of this expression,

$$\sigma_\ell(\cos\vartheta_e - \cos\vartheta) = \mu_\gamma U. \tag{2}$$

The implementation of similar free boundary problems but without contact line dissipation is well-known.[18] Existing studies with dynamic contact angles usually employ finite element arbitrary Lagrangian-Eulerian schemes,[19,20] which are mostly based on variational energetic arguments.

Thin-film equations are evolution equations for the film height h as shown in Fig. 2, for which moving contact lines have also been studied extensively. Here, the contact line singularity is somewhat concealed behind the mobility exponent $0 < \alpha < 3$ in

$$\partial_t h - \nabla\cdot\left[|h|^\alpha\nabla(-\Delta h + W'(h))\right] = 0, \tag{3}$$

as its value approaches $\alpha \to 3$. The classification of the singular behavior near moving contact lines has been performed

a)Electronic mail: peschka@wias-berlin.de

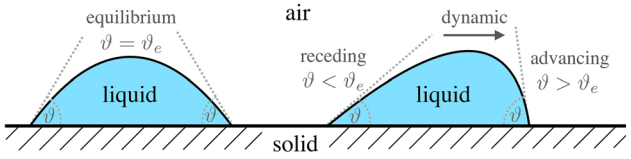

FIG. 1. Sketch of equilibrium angle ϑ_e for the stationary droplet and receding/advancing motion for the dynamic droplet.

both asymptotically[21] and rigorously.[22] This has led to different solution approaches, which we denote by *global* and by *supported* solutions for h. With global solutions we refer to non-negative functions $h : [0,T] \times \Sigma \to \mathbb{R}$ that are defined on a time-independent spatial domain Σ and can vanish on a subset $\omega \subset \Sigma$ of it. Corresponding nonnegativity preserving numerical schemes have been studied by Zhornitskaya and Bertozzi[23] and by Grün and Rumpf.[24] Supported solutions $h(t,\cdot) : \omega \to \mathbb{R}$ are defined on the time-dependent support set ω only. Without contact angle dynamics, i.e., $\vartheta = \vartheta_e$, this solution concept has been analyzed mathematically by Bertsch *et al.*[25] and by Knüpfer.[26] In particular, gradient flows have been employed to construct numerical algorithms for supported solutions describing thin films[27] and bilayers.[28] Energetic variational principles play an essential role for thin films,[28–32] as these allow us to apply certain mathematical tools and help us to ensure thermodynamic consistency for complex multiphysics problems.

The goal of this paper is to construct gradient flows for free boundary problems with models for dynamic contact angles. First, a gradient structure will be established for the Stokes flow and reduced to a thin-film model, for which efficient numerical algorithms are established. Therefore, in Sec. II, we introduce the Stokes gradient flow with free boundaries and provide the necessary definitions for the problem geometry, for the energy, and for the dissipation of viscous Newtonian fluids. This construction uses a dissipation term at the contact line, which then creates the contact angle model. We show that the Stokes flow with free boundaries and dynamic contact angle can be recovered using a Helmholtz-Rayleigh dissipation principle,[33] i.e., a gradient flow, using the so-called flow map as the state variable. In Sec. III, we perform a thin-film reduction, which is based on scaling arguments in the energy and the dissipation. Particular care is taken in treating all the terms at boundaries and contact lines correctly. We also derive a variational formulation of the thin-film model, which includes dissipation in the bulk (viscosity), at interfaces (Navier-slip),

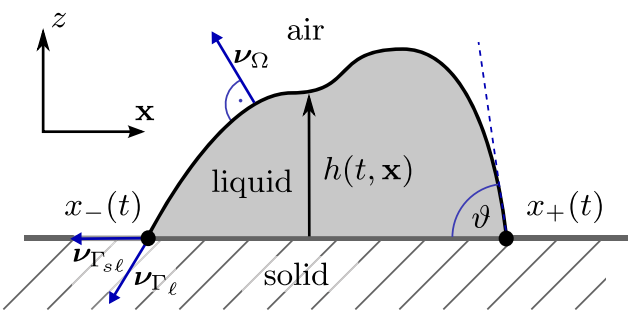

FIG. 2. Sketch of viscous liquid on a planar solid surface parametrized by h.

and at contact lines (dynamic contact angle). We discuss the numerical implementation of this model in detail in spatial dimension two. The generalization to higher dimensions is indicated where needed. Finally, we present an example showing gravity-driven moving droplets, where we highlight the effect of contact line dissipation and perform some robustness tests with the proposed numerical algorithm. The main novelty of this study is the construction and implementation of dynamic contact angle models for thin-films purely based on energetic arguments.

II. STOKES GRADIENT FLOW

The general idea of a gradient flow is to construct an abstract state space $q \in Q$ and a corresponding vector space of velocities $\dot q \in V$. The evolution of states $q(t)$ is then driven by an energy functional $\mathcal{E} : Q \to \mathbb{R}$. In the context of physical systems, this energy could be a thermodynamic potential for systems with diffusion and heat transport or it could be a potential energy for mechanical systems. Additionally, the construction requires a dissipation functional $\mathcal{D}(q,\cdot) : V \to \mathbb{R}$, which is convex and non-negative and in many cases is quadratic in the second argument. A quadratic dissipation $\mathcal{D}$ operates similar to a Riemannian metric and allows us to define gradients $\nabla_{\mathcal{D}}\mathcal{E} \in V$ by $\langle \mathrm{D}_{\dot q}\mathcal{D}(q,\nabla_{\mathcal{D}}\mathcal{E}),\dot p\rangle = \langle \mathrm{D}_q\mathcal{E}(q),\dot p\rangle$ for all $\dot p \in V$. The corresponding gradient flow then solves

$$\dot q(t) = -\nabla_{\mathcal{D}}\mathcal{E}(q(t)), \tag{4}$$

with energy $\frac{\mathrm{d}}{\mathrm{d}t}\mathcal{E}(q(t)) = \langle \mathrm{D}_q\mathcal{E},\dot q\rangle = -\langle \mathrm{D}_{\dot q}\mathcal{D}(q,\dot q),\dot q\rangle \le 0$ decreasing by construction. We deliberately employ the dot notation to indicate both membership $\dot p \in V$ and time-derivatives $\dot q = \frac{\partial}{\partial t}q$. The gradient flow is equivalent to the minimization of $\frac{1}{2}\mathcal{D}(q,\dot p) + \langle \mathrm{D}_q\mathcal{E},\dot p\rangle$ which is useful when considering alternative approaches and when considering constraints; e.g., see the work of Peletier.[34] The gradient flow construction applies to the irreversible dynamics where driving forces are entirely balanced by friction, as for the Stokes flow. Other examples of variational structures are Poisson or symplectic structures, e.g., Euler equations,[35] which are reversible and conserve energy. Nowadays, variational modeling has become an essential tool for the description of complex fluids.[36]

A. Geometry, flows, and functionals

We consider incompressible Newtonian liquids with density ρ with sufficiently large viscosity μ; i.e., the Reynolds number is small,

$$\mathrm{Re} = \frac{\rho UL}{\mu} \ll 1.$$

The motion of such a liquid layer Ω is parametrized,

$$\Omega(t) = \Big\{(\mathbf{x},z) \in \mathbb{R}^d : 0 < z < h(t,\mathbf{x})\Big\}, \tag{5a}$$

with a non-negative time-dependent function $h(t,\mathbf{x}) \ge 0$ describing the height of the liquid-air interface over the solid surface at $z = 0$ as shown in Fig. 2. Furthermore, we denote the time-dependent support of the function h with

$$\omega(t) = \{\mathbf{x} \in \mathbb{R}^{d-1} : h(t,\mathbf{x}) > 0\}, \tag{5b}$$

and the contact line is the set $\gamma(t) = (\partial\omega(t), 0)$. Due to its prominent appearance, $\boldsymbol{\nu} \in \mathbb{R}^{d-1}$ is used for the outer normal to ω on $\partial\omega$. Otherwise, the notation $\boldsymbol{\nu}_S$ refers to the outer

normal to S on ∂S. Later on, we consider the special case $d=2$ and ω is connected, so the support is a single interval written as $\omega(t) = (x_-(t), x_+(t))$ for $x_\pm(t) \in \mathbb{R}$ and correspondingly the contact line consists of the two points $\gamma(t) = \{(x_-(t), 0), (x_+(t), 0)\}$. In order to emphasize the relation of these sets and the state-space Q, one usually uses the concept of flow maps

$$q(t) = \big(\mathbf{X}(t,\cdot),\, Z(t,\cdot)\big) : \Omega_0 \to \Omega(t), \tag{6}$$

which are diffeomorphisms between $\Omega_0 = \Omega(0)$ and admissible shapes $\Omega = \Omega(t)$ at time t. Thereby q also maps any of the introduced domains at $t = 0$ to their shape at time $t > 0$. On the level of coordinates $\mathbf{y} \in \Omega_0$, we write $\mathbf{x} = \mathbf{X}(t, \mathbf{y}) \in \mathbb{R}^{d-1}$, $z = Z(t, \mathbf{y}) \in \mathbb{R}$ with $(\mathbf{x}, z) \in \Omega$. For fluids, the corresponding velocity field $\dot q(t) = (\dot{\mathbf{X}}(t,\cdot), \dot Z(t,\cdot)) : \Omega_0 \to \mathbb{R}^d$ is often expressed in Eulerian coordinates

$$\mathbf{u} = (\mathbf{u}_x, u_z) = \dot q \circ q^{-1} : \Omega \to \mathbb{R}^d.$$

In this sense, the Stokes or Navier-Stokes equation for the flow field $\mathbf{u}(t, \mathbf{x}, z)$ can be understood as an evolution equation for the flow map q. For incompressible liquids, this flow field is divergence free $\nabla \cdot \mathbf{u} = 0$. The driving energy consists of the parts $\mathcal{E} = \mathcal{E}_{\text{surf}} + \mathcal{E}_{\text{grav}}$, where

$$\mathcal{E}_{\text{surf}}(t) = \sigma_\ell |\Gamma_\ell(t)| + \sigma_{s\ell} |\Gamma_{s\ell}(t)|, \tag{7}$$

and $\Gamma_\ell(t) = \{(\mathbf{x}, z) : z = h(t, \mathbf{x}) > 0\}$ denotes the free liquid-air interface, the free solid-liquid interface is $\Gamma_{s\ell}(t) = (\omega(t), 0)$, and with $|\Gamma|$ we denote the measure of the set Γ. The surface tension coefficients are physical parameters with $\sigma_\ell = \sigma_{\text{liquid,air}} > 0$ and with $\sigma_{s\ell} = \sigma_{\text{solid,liquid}} - \sigma_{\text{solid,air}}$. By introducing the flow map, the energy depends on the state $\mathcal{E}(t) \equiv \mathcal{E}(q(t))$. Using (h, ω) to represent the flow map, one can rewrite the surface measures $|\Gamma_\ell|$ and $|\Gamma_{s\ell}|$ explicitly as

$$|\Gamma_\ell|(q) = \int_{\Gamma_\ell} \mathrm{d}s = \int_\omega \sqrt{1 + |\nabla h|^2}\, \mathrm{d}\mathbf{x}, \tag{8a}$$

$$|\Gamma_{s\ell}|(q) = \int_{\Gamma_{s\ell}} \mathrm{d}s = \int_\omega \mathrm{d}\mathbf{x} = |\omega| \overset{d=2}{=} x_+ - x_-. \tag{8b}$$

Throughout this paper, ∇ and $\nabla\cdot$ denote the gradient and divergence in both d and $d-1$ dimensions acting on all available spatial arguments, i.e., on $(\mathbf{x}, z)$ or on $\mathbf{x}$ as it should be clear from the context. Using the gravitational acceleration $g = 9.81\ \mathrm{m/s^2}$, we consider gravity in the x_1-direction as an energy defined as

$$\mathcal{E}_{\text{grav}}(q) = \int_\Omega \rho g x_1 \,\mathrm{d}\mathbf{x}\,\mathrm{d}z \equiv \rho g \int_\omega x_1 h \,\mathrm{d}\mathbf{x}. \tag{9}$$

For the model derivation, it is instructive to write all relevant friction mechanisms of this system. First, the dissipation for the bulk velocity is

$$\mathcal{D}_\Omega(\mathbf{u}) = \int_\Omega \boldsymbol{\tau}(\mathbf{u}) : \nabla \mathbf{u}\ \mathrm{d}\mathbf{x}\,\mathrm{d}z, \tag{10a}$$

where for Newtonian fluids the shear stress is of the form $\boldsymbol{\tau}(\mathbf{u}) = 2\mu_\Omega \mathbb{D}(\mathbf{u})$ with liquid viscosity $\mu_\Omega > 0$ and the symmetric gradient $\mathbb{D}(\mathbf{u}) = \frac{1}{2}(\nabla\mathbf{u} + \nabla\mathbf{u}^\top)$. Moving contact lines are known to produce logarithmic singularities for no-slip conditions, i.e., when we would simply set $\mathbf{u} = 0$ on $\Gamma_{s\ell}$. Instead, we just require impermeability $\mathbf{u} \cdot \mathbf{e}_z \equiv u_z = 0$ on $\Gamma_{s\ell}$ and introduce the dissipation at the solid-liquid interface

$$\mathcal{D}_\omega(\mathbf{u}) = \int_{\Gamma_{s\ell}} \mu_\omega \mathbf{u}_\mathbf{x}^2 \,\mathrm{d}s, \tag{10b}$$

where $\mu_\omega \geq 0$ is related to the well-known Navier-slip length b via $\mu_\omega = \mu_\Omega / b$. Consequently, we also introduce a quadratic dissipation mechanism at the contact line γ, which reads

$$\mathcal{D}_\gamma(\mathbf{u}) = \int_\gamma \mu_\gamma \mathbf{u}_\mathbf{x}^2 \,\mathrm{d}\gamma \overset{d=2}{=} \mu_\gamma (\dot x_-^2 + \dot x_+^2), \tag{10c}$$

where the latter reformulation is only meaningful for $d = 2$, and $\dot x_\pm = \frac{d}{dt} x_\pm$ denotes the contact line velocity and $\mu_\gamma \geq 0$ is the friction coefficient. For higher dimensions $d > 2$, it can make sense to further decompose the contact line dissipation into two contributions $\mathcal{D}_\gamma(\mathbf{u}) = \int_\gamma \mu_\perp (\mathbf{u}_\mathbf{x} \cdot \boldsymbol{\nu})^2 + \mu_\parallel ([1 - \boldsymbol{\nu}\boldsymbol{\nu}^\top]\mathbf{u}_\mathbf{x})^2 \,\mathrm{d}\gamma$. When all dissipation terms are collected, the total dissipation is

$$\mathcal{D}(\mathbf{u}) = \mathcal{D}_\Omega(\mathbf{u}) + \mathcal{D}_\omega(\mathbf{u}) + \mathcal{D}_\gamma(\mathbf{u}), \tag{10d}$$

which is a positive quadratic functional for incompressible flow fields $\mathbf{u}$. The dependence of $\mathcal{D} : Q \times V \to \mathbb{R}$ on the state q through the shape of Ω, ω, γ is not stated explicitly as an argument. The evolution of the domain, which can be represented by (h, ω), is restricted by the constraints of incompressibility and by the kinematic condition,

$$\dot h + \nabla \cdot \left(\int_0^h \mathbf{u}_\mathbf{x} \,\mathrm{d}z \right) = 0. \tag{11}$$

In addition to the flow maps, this allows us to define auxiliary states (h, ω) and velocities $(\dot h, \dot{\mathbf{x}})$, where we denote with $\dot{\mathbf{x}} : \gamma \to \mathbb{R}^{d-1}$ the restriction of $\mathbf{u}_\mathbf{x}$ to γ.

B. Gradient flow construction

Using the formal gradient flow recipe, we obtain the Stokes free boundary problem via the constrained minimization problem

$$\mathbf{u}(t,\cdot) = \operatorname*{argmin}_{\mathbf{v} \in V} \left(\tfrac{1}{2}\mathcal{D}(\mathbf{v}) + \langle \mathrm{D}_q \mathcal{E}, \mathbf{v} \rangle \right), \tag{12}$$

for which differentiation at $\mathbf{u}$ in the direction of $\mathbf{v}$ results in the weak formulation of the Euler-Lagrange equation $a(\mathbf{u},\, \mathbf{v}) = f(\mathbf{v})$ for all $\mathbf{v} \in V$. The bilinear form $a(\mathbf{u}, \mathbf{v}) := \frac{1}{2}\langle \mathrm{D}_{\dot q} \mathcal{D}(\mathbf{u}), \mathbf{v} \rangle$ is

$$\begin{aligned} a(\mathbf{u}, \mathbf{v}) = &\int_\Omega 2\mu_\Omega \mathbb{D}(\mathbf{u}) : \mathbb{D}(\mathbf{v}) \,\mathrm{d}\mathbf{x}\,\mathrm{d}z \\ &+ \int_{\Gamma_{s\ell}} \mu_\omega \mathbf{u}_\mathbf{x} \cdot \mathbf{v}_\mathbf{x} \,\mathrm{d}s \quad + \int_\gamma \mu_\gamma\, \dot{\mathbf{x}} \cdot \mathbf{v}_\mathbf{x} \,\mathrm{d}\gamma, \end{aligned} \tag{13a}$$

and the linear functional is $f(\mathbf{v}) := \langle -\mathrm{D}_q \mathcal{E}, \mathbf{v} \rangle$, where $\mathrm{D}_q \mathcal{E} = \mathrm{D}_q \mathcal{E}_{\text{surf}} + \mathrm{D}_q \mathcal{E}_{\text{grav}}$. For the surface energy using the surface divergence $\bar\nabla\cdot$ and the tangential gradient $\bar\nabla$, this can be written as

$$\langle \mathrm{D}_q \mathcal{E}_{\text{surf}}, \mathbf{v} \rangle = \sigma_\ell \int_{\Gamma_\ell} \bar\nabla \cdot \mathbf{v} \,\mathrm{d}s + \sigma_{s\ell} \int_{\Gamma_{s\ell}} \bar\nabla \cdot \mathbf{v} \,\mathrm{d}s. \tag{13b}$$

In order to (formally) reconstruct the strong form of the differential equation, we use integration by parts on curved surfaces

$$\int_\Gamma \bar\nabla \cdot \mathbf{v} \,\mathrm{d}s = -(d-1) \int_\Gamma \kappa \boldsymbol{\nu}_\Omega \cdot \mathbf{v} \,\mathrm{d}s + \int_{\partial\Gamma} \mathbf{v} \cdot \boldsymbol{\nu}_\Gamma \,\mathrm{d}\gamma,$$

where κ denotes the signed mean curvature (see Appendix A), $\boldsymbol{\nu}_\Omega$ is the outer normal of Ω on the free surface $\Gamma \subset \partial\Omega$, $\boldsymbol{\nu}_\Gamma$ is the outer normal of Γ on $\partial\Gamma$, and finally $\mathrm{d}s$ and $\mathrm{d}\gamma$ are the integration measures of Γ and $\partial\Gamma$. Note that due to impermeability $\mathbf{v}\cdot\mathbf{e}_z = 0$ only the term at $\partial\Gamma_{s\ell}$ contributes from $\mathrm{D}_q|\Gamma_{s\ell}|$ so that $\langle \mathrm{D}_q\mathcal{E}_{\mathrm{surf}}, \mathbf{v}\rangle = -(d-1)\sigma_\ell \int_{\Gamma_\ell} \kappa\boldsymbol{\nu}_\Omega\cdot\mathbf{v}\,\mathrm{d}s + \int_\gamma \mathbf{f}_\gamma\cdot\mathbf{v}\,\mathrm{d}\gamma$ with the force assigned to the contact line defined as $\mathbf{f}_\gamma = (\sigma_\ell\boldsymbol{\nu}_{\Gamma_\ell} + \sigma_{s\ell}\boldsymbol{\nu}_{\Gamma_{s\ell}})$. Sometimes $\mathbf{f}_\gamma$ is referred to as uncompensated Young force (see Appendix C). Finally, gravity can be included by using Reynold's transport theorem to obtain

$$\begin{aligned}\langle \mathrm{D}_q\mathcal{E}_{\mathrm{grav}}, \mathbf{v}\rangle &= \int_\Omega \nabla\cdot(\rho g x_1\mathbf{v})\,\mathrm{d}\mathbf{x}\,\mathrm{d}z\\ &= \int_{\Gamma_\ell} \rho g x_1\,\mathbf{v}\cdot\boldsymbol{\nu}\,\mathrm{d}s. \end{aligned}\tag{13c}$$

In total, this produces the strong form of the partial differential equation (PDE) for the unknown velocity $\mathbf{u}(t,\cdot) : \Omega(t) \to \mathbb{R}^d$ so that

$$\nabla\cdot\boldsymbol{\tau}(\mathbf{u}) = \nabla(p+\rho g x_1) \quad \text{in } \Omega(t), \tag{14a}$$
$$\nabla\cdot\mathbf{u} = 0 \quad \text{in } \Omega(t), \tag{14b}$$
$$\mathbf{t}\cdot(\boldsymbol{\tau}\cdot\boldsymbol{\nu}_\Omega + \mu_\omega\mathbf{u}) = 0 \quad \text{on } \Gamma_{s\ell}(t), \tag{14c}$$
$$u_z = 0 \quad \text{on } \Gamma_{s\ell}(t), \tag{14d}$$
$$(-p\mathbb{I}+\boldsymbol{\tau})\cdot\boldsymbol{\nu}_\Omega = (d-1)\sigma_\ell\kappa\boldsymbol{\nu}_\Omega \quad \text{on } \Gamma_\ell(t), \tag{14e}$$
$$\mu_\gamma\dot{\mathbf{x}} = -\mathbb{P}_{\mathbf{x}}\mathbf{f}_\gamma \quad \text{at } \gamma(t), \tag{14f}$$

where the pressure $p(t,\cdot) : \Omega(t) \to \mathbb{R}$ is added as a Lagrange multiplier to account for the incompressibility in the constrained minimization (12) and we use $\mathbb{P}_{\mathbf{x}} = (\mathbb{I}_{d-1}, 0) \in \mathbb{R}^{(d-1)\times d}$ to project the force into the $(d-1)$-dimensional $\mathbf{x}$-plane. Then, the domain $\Omega(t)$ evolves according to the kinematic condition (11). The mathematical analysis of such a problem without contact lines is by Beale.[37] The discretization of such models using finite elements was discussed by Bänsch[18] and Montefuscolo.[20] For the latter, the variational formulation was proposed by Ren and E.[12] For an introduction to variational modeling and gradient flows, and, in particular, the mathematical equivalence of different energetic variational principles, we refer to the lecture notes by Peletier.[34] A typical solution of this Stokes free boundary problem is shown in Fig. 3 (Multimedia view). This solution was computed using Taylor-Hood P_2/P_1 finite elements using the Laplace-Beltrami technique to introduce capillary forces,[18] where an extra term in the variational formulation introduces the contact line dissipation.

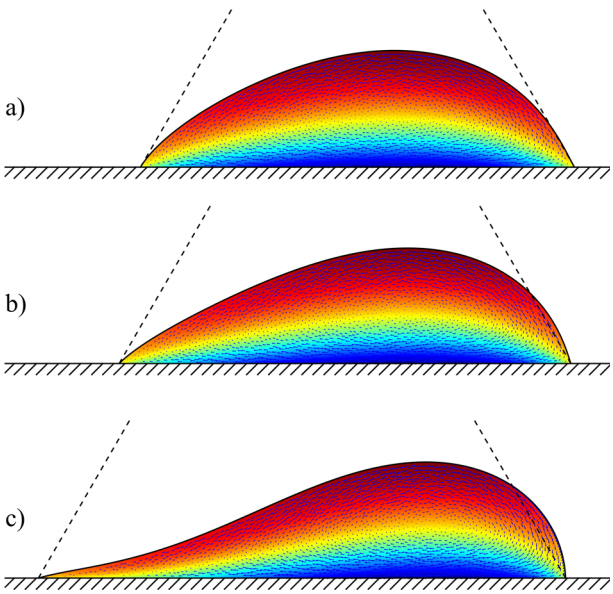

FIG. 3. Drop evolution for the Stokes free boundary problem with the contact angle model with $\sigma_\ell = 1$, $\vartheta_e = \pi/3$, $\mu_\Omega = 1$, and $\mu_\Gamma = 4$ and with contact angle model (a) $\mu_\gamma = 0$ (equilibrium), (b) $\mu_\gamma = 1$, (c) $\mu_\gamma = 8$, where arrows show flow in a comoving frame and shading shows its magnitude in a fixed frame. The dashed lines show the equilibrium contact angle. Multimedia view: https://doi.org/10.1063/1.5040985.1

III. THIN-FILM MODELS

A. Non-dimensionalization

Now we discuss, how the free boundary problem (14) is reduced to a thin-film type model for the film height h and its support set ω. Particular care is taken in the treatment of boundary and interface terms. A cornerstone of the lubrication model is the non-dimensionalization of lengths, of velocities, and of time,

$$\mathbf{x} = L\tilde{\mathbf{x}}, \quad z = \varepsilon L\tilde{z}, \quad \mathbf{u}_{\mathbf{x}} = U\tilde{\mathbf{u}}_{\mathbf{x}}, \quad u_z = \varepsilon U\tilde{u}_z, \quad t = T\tilde{t},$$

for length L, horizontal velocity U, and a time scale defined $T = L/U$. We introduced the small parameter $0 < \varepsilon \ll 1$ that will reflect the small slope assumption of the thin-film model reduction. The preceding problem statement contains 6 physical parameters $(\mu_\Omega, \mu_\omega, \mu_\gamma, \sigma_\ell, \sigma_{s\ell}, \rho g) \in \mathbb{R}^6$ and the initial data $\Omega(t=0) \subset \mathbb{R}^d$ that solutions depend on. Now we define the scales introduced above to reduce the set of physical parameters to a minimal set of non-dimensional parameters. Therefore, we expand the bilinear form $\tilde{\mathbf{u}}$ and for brevity omit writing lower order terms (l.o.t.)

$$\begin{aligned}\frac{a(\mathbf{u},\mathbf{v})}{L^{d-2}U^2} = \frac{\mu_\Omega}{\varepsilon}\int_\Omega (\partial_{\tilde{z}}\tilde{\mathbf{u}}_{\mathbf{x}})(\partial_{\tilde{z}}\tilde{\mathbf{v}}_{\mathbf{x}})\,\mathrm{d}\tilde{\mathbf{x}}\,\mathrm{d}\tilde{z} + \frac{\mu_\Omega L}{b}\int_{\Gamma_{s\ell}} \tilde{\mathbf{u}}_{\mathbf{x}}\cdot\tilde{\mathbf{v}}_{\mathbf{x}}\,\mathrm{d}\tilde{s}\\ + \mu_\gamma\int_\gamma \tilde{\mathbf{u}}_{\mathbf{x}}\cdot\tilde{\mathbf{v}}_{\mathbf{x}}\,\mathrm{d}\tilde{\gamma} + \text{l.o.t.},\end{aligned}$$

where all three terms contribute to the leading order if $b \sim \varepsilon L$ and $\mu_\gamma \sim \varepsilon^{-1}\mu_\Omega$ as $\varepsilon \to 0$. Therefore, we denote by $\tilde{b} = b/(\varepsilon L)$ and $\tilde{\mu}_\gamma = \varepsilon\tilde{b}\mu_\gamma/\mu_\Omega$ the rescaled non-dimensional parameters. Having $\tilde{b} \sim 1$ is realistic in some microfluidic settings since slip-lengths between nanometers and micrometers have been observed experimentally. The contact line singularity is usually resolved at microscopic length scales much smaller than L, which leads to an apparent contact line friction as predicted by Cox and Voinov. However, μ_γ might very well be an intrinsic physical parameter on its own right. For the moment, we consider the energy contribution from (8a) and perform the thin-film reduction by expanding

$$\begin{aligned}|\Gamma_\ell| &= \int_\omega \sqrt{1+|\nabla h|^2}\,\mathrm{d}\mathbf{x}\\ &= L^{d-1}\int_\omega \Big(1+\frac{\varepsilon^2}{2}|\tilde{\nabla}\tilde{h}|^2\Big)\,\mathrm{d}\tilde{\mathbf{x}} + \text{l.o.t.},\end{aligned}$$

for the first two non-trivial terms, as this is necessary to give a consistent model reduction. Then the derivative of this functional is

$$\frac{\langle \mathrm{D}_q|\Gamma_\ell|,\mathbf{v}\rangle}{L^{d-2}U} = \int_\omega \varepsilon^2\tilde\nabla\tilde h\cdot\tilde\nabla\dot{\tilde h}_{\mathbf{v}}\,\mathrm{d}\tilde{\mathbf{x}} + \int_\gamma \Big(1+\frac{\varepsilon^2}{2}|\tilde\nabla\tilde h|^2\Big)\tilde{\mathbf{v}}_{\mathbf{x}}\cdot\boldsymbol{\nu}\,\mathrm{d}\tilde\gamma + \text{l.o.t.},$$

where we associate $\dot h_{\mathbf{v}} + \nabla\cdot\int_0^h \mathbf{v}_{\mathbf{x}}\,\mathrm{d}z = 0$ to any $\mathbf{v}\in V$ as in (11) and $\tilde\nabla$ acts on $\tilde{\mathbf{x}}$. In order to arrive at this derivative, one needs to use Reynold's transport theorem, to take into account the derivative with respect to the motion of the support. Using the definition of $\dot h_{\mathbf{v}}$, we can rewrite the first term as

$$\begin{aligned}\int_\omega \tilde\nabla\tilde h\cdot\tilde\nabla\dot{\tilde h}_{\mathbf{v}}\,\mathrm{d}\tilde{\mathbf{x}} &= -\int_\omega(\tilde\Delta\tilde h)\dot{\tilde h}_{\mathbf{v}}\,\mathrm{d}\tilde{\mathbf{x}} + \int_\gamma \dot{\tilde h}_{\mathbf{v}}\tilde\nabla_{\boldsymbol{\nu}}\tilde h\,\mathrm{d}\tilde\gamma\\ &= \int_\omega \tilde\Delta\tilde h\Big[\tilde\nabla\cdot\int_0^h\tilde{\mathbf{v}}_{\mathbf{x}}\,\mathrm{d}\tilde z\Big]\mathrm{d}\tilde{\mathbf{x}} + \int_\gamma \dot{\tilde h}_{\mathbf{v}}\tilde\nabla_{\boldsymbol{\nu}}\tilde h\,\mathrm{d}\tilde\gamma\\ &= \int_\Omega -\tilde\nabla\tilde\Delta\tilde h\cdot\tilde{\mathbf{v}}_{\mathbf{x}}\,\mathrm{d}\tilde{\mathbf{x}}\,\mathrm{d}\tilde z + \int_\gamma \dot{\tilde h}_{\mathbf{v}}\tilde\nabla_{\boldsymbol{\nu}}\tilde h\,\mathrm{d}\tilde\gamma,\end{aligned}$$

where the last term on the boundary in the integration-by-parts vanished because $\int_0^h\tilde{\mathbf{v}}_{\mathbf{x}}\,\mathrm{d}\tilde z\equiv 0$ on γ. Since $h\equiv 0$ on γ, we have $\dot h_{\mathbf{v}} + \mathbf{v}_{\mathbf{x}}\cdot\nabla h = 0$ for the convective derivative. This allows us to transform the last term into

$$\int_\gamma \dot{\tilde h}_{\mathbf{v}}\tilde\nabla_{\boldsymbol{\nu}}\tilde h\,\mathrm{d}\tilde\gamma = \int_\gamma -\tilde{\mathbf{v}}_{\mathbf{x}}\cdot\boldsymbol{\nu}|\tilde\nabla\tilde h^2|\,\mathrm{d}\tilde\gamma.$$

For each of the surfaces, we get the derivative to be

$$\begin{aligned}\frac{\langle \mathrm{D}_q|\Gamma_\ell|,\mathbf{v}\rangle}{L^{d-2}U} &= \int_\Omega -\varepsilon^2\tilde\nabla\tilde\Delta\tilde h\cdot\tilde{\mathbf{v}}_{\mathbf{x}}\,\mathrm{d}\tilde{\mathbf{x}}\,\mathrm{d}\tilde z + \int_\gamma(1-\tfrac{\varepsilon^2}{2}|\tilde\nabla\tilde h|^2)\tilde{\mathbf{v}}_{\mathbf{x}}\cdot\boldsymbol{\nu}\,\mathrm{d}\tilde\gamma + \text{l.o.t.},\\ \frac{\langle \mathrm{D}_q|\Gamma_{s\ell}|,\mathbf{v}\rangle}{L^{d-2}U} &= \int_\gamma \tilde{\mathbf{v}}_{\mathbf{x}}\cdot\boldsymbol{\nu}\,\mathrm{d}\tilde\gamma\end{aligned}$$

so that for the derivative of the surface energy we get

$$\frac{\langle \mathrm{D}_q\mathcal{E}_{\mathrm{surf}},\mathbf{v}\rangle}{L^{d-2}U} = \int_\Omega -\varepsilon^2\sigma_\ell\tilde\nabla\tilde\Delta\tilde h\cdot\tilde{\mathbf{v}}_{\mathbf{x}}\,\mathrm{d}\tilde{\mathbf{x}}\,\mathrm{d}\tilde z + \int_\gamma\Big[\sigma_{s\ell}+\sigma_\ell(1-\tfrac{\varepsilon^2}{2}|\tilde\nabla\tilde h|^2)\Big]\tilde{\mathbf{v}}_{\mathbf{x}}\cdot\boldsymbol{\nu}\,\mathrm{d}\tilde\gamma + \text{l.o.t.}$$

For all terms to contribute at the same order, we require $\sigma_\ell+\sigma_{s\ell}\sim\varepsilon^2$. This lets us fix ε so that

$$\varepsilon^2 = \frac{\sigma_\ell+\sigma_{s\ell}}{\sigma_\ell} \equiv 1-\cos\vartheta_e \tag{15a}$$

is indeed small, when the contact angle is small. Having the property $0<\varepsilon\ll 1$ is necessary to ensure the consistency of the asymptotic scaling that later leads to the thin-film model reduction. Similarly we rescale the gravitational energy and get

$$\frac{\langle \mathrm{D}_q\mathcal{E}_{\mathrm{grav}},\mathbf{v}\rangle}{\varepsilon\rho|g|L^dU} = \mathrm{sign}(g)\int_\Omega \mathbf{e}_{x_1}\cdot\tilde{\mathbf{v}}_{\mathbf{x}}\,\mathrm{d}\tilde{\mathbf{x}}\,\mathrm{d}+\text{l.o.t.}$$

In order to fix the velocity scale, we balance the dissipation in the Navier-slip contribution with the surface energy and get

$$\mathrm{Ca} = \frac{\mu_\Omega U}{\sigma_\ell} = \varepsilon^3\tilde b, \tag{15b}$$

with the capillary number Ca. Finally, we can determine the length scale L by balancing surface and gravitational energy and obtain

$$\mathrm{Bo} = \frac{|\rho|gL^2}{\sigma_\ell} = 4\varepsilon, \tag{15c}$$

with the Bond number Bo and where the factor 4 is the convention of this paper. After this non-dimensionalization, the non-dimensional parameters are

$$\varepsilon^2 = 1-\cos\vartheta_e,\qquad \tilde b = \frac{b}{\varepsilon L},\qquad \tilde\mu = \frac{\varepsilon\tilde b\mu_\gamma}{\mu_\Omega},$$

and initial data $\tilde h(\tilde t=0,\tilde x) = (\varepsilon L)^{-1}h(t=0,L\tilde x)$.

B. Thin-film model reduction

We perform the thin-film model reduction by first assuming that the solution $\tilde{\mathbf{u}}$ has a formal asymptotic expansion

$$\begin{aligned}\tilde{\mathbf{u}}(t,\mathbf{x},z) &= \tilde{\mathbf{u}}^0(t,\mathbf{x},z)+\varepsilon\tilde{\mathbf{u}}^1(t,\mathbf{x},z)+\mathcal{O}(\varepsilon^2),\\ \tilde h(t,\mathbf{x}) &= \tilde h^0(t,\mathbf{x})+\varepsilon\tilde h^1(t,\mathbf{x})+\mathcal{O}(\varepsilon^2).\end{aligned}$$

We plug this expansion into the derived expressions for energy and dissipation and only collect the leading order equation for $\tilde{\mathbf{u}}^0$ and $\tilde h^0(t,\mathbf{x})$. Dropping the tilde and the superscript "0" everywhere, one ends up with

$$\begin{aligned} b\int_\omega\Big(\int_0^h -\partial_{zz}\mathbf{u}_{\mathbf{x}}\mathbf{v}_{\mathbf{x}}\,\mathrm{d}z\Big) + \Big(\partial_z\mathbf{u}_{\mathbf{x}}\mathbf{v}_{\mathbf{x}}\Big)_0^h\,\mathrm{d}\mathbf{x}&\\ + \int_{\Gamma_{s\ell}}\mathbf{u}_{\mathbf{x}}\cdot\mathbf{v}_{\mathbf{x}}\,\mathrm{d}\mathbf{x} + \int_\gamma\mu_\gamma\,\dot{\mathbf{x}}\cdot\mathbf{v}_{\mathbf{x}}\mathrm{d}\gamma&\\ = \int_\Omega\nabla\Delta h\cdot\mathbf{v}_{\mathbf{x}}\,\mathrm{d}\mathbf{x}\,\mathrm{d}z - \int_\gamma(1-\tfrac12|\nabla h|^2)\mathbf{v}_{\mathbf{x}}\cdot\boldsymbol{\nu}\,\mathrm{d}\gamma&\\ - \int_\Omega 4\,\mathrm{sign}(g)\mathbf{e}_x\cdot\mathbf{v}_{\mathbf{x}}\,\mathrm{d}\mathbf{x}\,\mathrm{d}z,&\end{aligned}$$

which needs to hold for all test functions $\mathbf{v}\in V$. We can integrate this equation for $\mathbf{u}_{\mathbf{x}}(t,\mathbf{x},z)$ in z and obtain the following polynomial in z with $\mathbf{x}$-dependent coefficients

$$\mathbf{u}_{\mathbf{x}} = \frac{z^2}{2b}\nabla[-\Delta h+4x_1]+c_1z+c_0, \tag{16}$$

where $c_0(t,\mathbf{x})$, $c_1(t,\mathbf{x})$ are determined by the boundary conditions $\partial_z\mathbf{u}_{\mathbf{x}}=0$ at $z=h$ and $b\,\partial_z\mathbf{u}_{\mathbf{x}}+\mathbf{u}_{\mathbf{x}}=0$ at $z=0$ implied by the boundary terms before. Without loss of generality, we assumed $\mathrm{sign}(g)=-1$, and solutions with the different sign are obtained by reflection along the x_1-axis. At the contact line γ, one obtains the law

$$\mu_\gamma\,\dot{\mathbf{x}} = \Big(\frac12|\nabla h|^2-1\Big)\boldsymbol{\nu} \tag{17}$$

so that the contact line is advancing, receding, or stationary for $|\nabla h|>\sqrt2$, $|\nabla h|<\sqrt2$, or $|\nabla h|=\sqrt2$, respectively. In the thin-film approximation, we have contact angles $\vartheta\sim\varepsilon\nabla h$ and the equilibrium contact angle $\vartheta_{\mathrm{e}}=\varepsilon\sqrt2$ so that we have a dynamic contact angle in the slightly more familiar form

$$\mu_\gamma\,\dot{\mathbf{x}} = \frac{1}{2\varepsilon^2}\Big(\vartheta^2-\vartheta_{\mathrm{e}}^2\Big)\boldsymbol{\nu}. \tag{18}$$

The last step is to insert the explicit expression for $\mathbf{u}_\mathbf{x}$ into the kinematic condition (11). This returns the degenerate, fourth-order parabolic equation

$$\dot{h} = \nabla \cdot \Big(m(h)\, \nabla \left(-\Delta h + 4x_1\right)\Big), \tag{19a}$$

$$\mu_\gamma\, \dot{\mathbf{x}} = \left(\frac{1}{2}|\nabla h|^2 - 1\right)\boldsymbol{\nu}, \tag{19b}$$

for the height h and the boundary $\mathbf{x}$ alone. Additionally we have the constraint $\dot{h} + \dot{\mathbf{x}} \cdot \nabla h = 0$ on γ. The mobility m encodes the dissipation mechanism in the bulk and at the interface, where our integration gives

$$m(h) = \frac{h^3}{3b} + h^2, \tag{19c}$$

and b encodes the rescaled slip-length that we introduced before. Employing the rescaled parametrization in the original surface energy gives

$$\begin{aligned}
\mathcal{E}_{\text{surf}} &= L^{d-1} \int_\omega \sigma_\ell \sqrt{1 + \varepsilon^2 |\nabla h|^2} + \sigma_{s\ell}\, \mathrm{d}\mathbf{x} \\
&= L^{d-1} \int_\omega \sigma_\ell \left(1 + \frac{\varepsilon^2}{2}|\nabla h|^2\right) + \sigma_{s\ell}\, \mathrm{d}\mathbf{x} + \text{l.o.t.} \\
&\approx \varepsilon^2 L^{d-1} \sigma_\ell \int_\omega \left(1 + \frac{1}{2}|\nabla h|^2\right) \mathrm{d}\mathbf{x} \\
&=: \varepsilon^2 L^{d-1} \sigma_\ell\, \mathcal{E}_{\text{tf}}^{\text{surf}},
\end{aligned}$$

where in the last step we used the previous definition of $\varepsilon^2 = (\sigma_\ell + \sigma_{s\ell})/\sigma_\ell$ to define the thin-film surface energy $\mathcal{E}_{\text{tf}}^{\text{surf}}$. Similarly, we are including gravity using the term $\mathcal{E}_{\text{tf}}^{\text{grav}} = \int_\omega W(h;\mathbf{x})\, \mathrm{d}\mathbf{x}$ with $W(h, \mathbf{x}) = 4hx_1$ in the thin-film energy $\mathcal{E}_{\text{tf}} = \mathcal{E}_{\text{tf}}^{\text{surf}} + \mathcal{E}_{\text{tf}}^{\text{grav}}$. Note that gravity in the x-direction corresponds to fluid sliding down a vertical wall. To account for an angle, one would need to modify $W(h, \mathbf{x}) = 4hx_1 + \beta h^2$. Since we have $W(0; \mathbf{x}) \equiv 0$, this term does not contribute to the contact angle dynamics. The variational formulation of the thin-film model is discussed now in more detail.

C. Variational thin-film model

Let us consider the simpler problem of finding the velocities $\dot{h}$ with $\dot{h} : \omega \to \mathbb{R}$ that solve a thin-film model in the weak form on a *fixed* domain ω and strictly positive h. The corresponding variational formulation requires the introduction of an additional variable $\pi : \omega \to \mathbb{R}$, which is related to a given $\dot{h}$ through the degenerate elliptic equation

$$\dot{h} - \nabla \cdot (m(h) \nabla \pi) = 0, \tag{20}$$

with homogeneous natural boundary conditions $m\boldsymbol{\nu} \cdot \nabla \pi = 0$. Then, the thin-film model on a fixed domain has a gradient structure with the dissipation,

$$\mathcal{D}_{\text{tf}}(\dot{h}_v) = \int_\omega m(h) |\nabla \pi|^2\, \mathrm{d}\mathbf{x}, \tag{21a}$$

and with the driving thin-film energy

$$\mathcal{E}_{\text{tf}}(h) = \int_\omega 1 + \frac{1}{2}|\nabla h|^2 + W(h;\mathbf{x})\, \mathrm{d}\mathbf{x}. \tag{21b}$$

The evolution of the height $h(t, \mathbf{x})$ is again governed by a constrained minimization problem

$$\dot{h}(t, \cdot) = \operatorname*{argmin}_{\dot{h}_v \in V} \left(\frac{1}{2}\mathcal{D}_{\text{tf}}(\dot{h}_v) + \langle \mathrm{D}_h \mathcal{E}_{\text{tf}}, \dot{h}_v \rangle\right), \tag{22}$$

similar to the one in (12). The corresponding Euler-Lagrange equation of this saddle-point problem can be written in the block form

$$\begin{pmatrix} 0 & 0 & M^* \\ 0 & D & D^* \\ M & D & 0 \end{pmatrix} \begin{pmatrix} \dot{h} \\ \pi \\ \lambda \end{pmatrix} = \begin{pmatrix} -Sh - M\partial_h W \\ 0 \\ 0 \end{pmatrix} \tag{23}$$

and where $\lambda : \omega \to \mathbb{R}$ is the Lagrange multiplier enforcing (20) and the operators M, D, S are defined as

$$\langle v, Mw \rangle = \int_\omega v w\, \mathrm{d}\mathbf{x}, \tag{24a}$$

$$\langle v, D\, w \rangle = \int_\omega m(h) \nabla v \cdot \nabla w\, \mathrm{d}\mathbf{x}, \tag{24b}$$

$$\langle v, S\, w \rangle = \int_\omega \nabla v \cdot \nabla w\, \mathrm{d}\mathbf{x}, \tag{24c}$$

and map function spaces for $\dot{h}$, π, λ into appropriate dual function spaces. We presume that the operators D, M, S are self-adjoint. In the 3×3 block matrix on the left side of (23), the upper-left 2×2 block constitutes the contribution from the dissipation, whereas the remaining parts result from the constraints. The first line of the block operator (23) implies $\lambda = \Delta h - \partial_h W$, whereas the second line implies basically $\pi = -\lambda = \delta \mathcal{E}_{\text{tf}}/\delta h$ so that the third line $\dot{h} - \nabla \cdot (m \nabla \pi) = 0$ produces the thin-film equation as in (3) or in (19a) as

$$\dot{h} - \nabla \cdot (m(h) \nabla \pi) = 0, \quad \pi = -\Delta h + \partial_h W(h;\mathbf{x}). \tag{25}$$

We introduced the saddle-point problem (23) in preparation for the more complex gradient structure with moving contact lines, where additional bulk-interface coupling terms are required. Now we will state the gradient form of the model with dynamic contact angle.

As before, in the presence of a moving contact line, h is supported only on the set $\omega(t)$ with the contact line defined as the set $\gamma(t) = \partial\omega(t)$. Let $\mathbf{x}(t) \in \gamma(t)$ be a point on the contact line, then $h(t, \mathbf{x}(t)) \equiv 0$ for all t and consequently

$$\tfrac{\mathrm{d}}{\mathrm{d}t} h(t, \mathbf{x}(t)) = \dot{h}(t, \mathbf{x}(t)) + \dot{\mathbf{x}}(t) \cdot \nabla h\big(t, \mathbf{x}(t)\big) = 0. \tag{26}$$

Since (26) does not depend on the parameterization, it is justified to simply write $\dot{h} + \dot{\mathbf{x}} \cdot \nabla h = 0$ with $\dot{\mathbf{x}} : \gamma \to \mathbb{R}^d$ the contact line speed introduced before. This condition relates the normal component of $\dot{\mathbf{x}}$ to the Eulerian time derivative $\dot{h}$ of the height. Analogous to the gradient structure of the Stokes model, we understand $q = (h, \omega)$ as the general state with velocities $\dot{q} = (\dot{h}, \dot{\mathbf{x}})$. The corresponding dissipation for the thin-film model analogous to (21a) but with contact angle dynamics is

$$\mathcal{D}_{\text{tf}}(\dot{q}) = \int_\omega m(h) |\nabla \pi|^2\, \mathrm{d}\mathbf{x} + \int_\gamma \mu_\gamma \dot{\mathbf{x}}^2\, \mathrm{d}\gamma \tag{27}$$

and the driving thin-film energy $\mathcal{E}_{\text{tf}}$ from (21b). Since now the support can change, we use Reynolds' transport theorem to include variations of the energy (21b) with respect to the shape of ω via

$$\begin{aligned}
\langle \mathrm{D}_q \mathcal{E}_{\text{tf}}, \dot{q} \rangle = &\int_\omega \nabla h \cdot \nabla \dot{h} + \partial_h W(h;\mathbf{x}) \dot{h}\, \mathrm{d}\mathbf{x} \\
&+ \int_\gamma \left(1 + \tfrac{1}{2}|\nabla h|^2\right)(\dot{\mathbf{x}} \cdot \boldsymbol{\nu})\, \mathrm{d}\gamma.
\end{aligned}$$

In the standard thin-film model, we only have to enforce the constraint $\dot h - \nabla\cdot(m\nabla\pi) = 0$ in ω using a multiplier $\lambda : \omega \to \mathbb{R}$, whereas now we additionally have to enforce $\dot h + \dot{\mathbf{x}}\cdot\nabla h = 0$ on the contact line γ with a multiplier $\kappa : \gamma \to \mathbb{R}$. Additionally, the resulting linear system has a potential ambiguity with respect to adding a constant to π, which we resolve by adding a constraint $\int\pi\,\mathrm{d}\mathbf{x} = 0$ with a multiplier $\rho \in \mathbb{R}$. Therefore we seek $u = (\dot h, \pi, \dot{\mathbf{x}}, \lambda, \kappa, \rho)^\top$ solving the corresponding constrained minimization problem leading to $Au = -b$, where $A : X \to X^*$ is defined as

$$Au = \begin{pmatrix} \cdot & \cdot & \cdot & M^* & M_\gamma^* & \cdot \\ \cdot & D & \cdot & D^* & \cdot & M_0^* \\ \cdot & \cdot & D_\gamma & \cdot & C_\gamma^* & \cdot \\ M & D & \cdot & \cdot & \cdot & \cdot \\ M_\gamma & \cdot & C_\gamma & \cdot & \cdot & \cdot \\ \cdot & M_0 & \cdot & \cdot & \cdot & \cdot \end{pmatrix} \begin{pmatrix} \dot h \\ \pi \\ \dot{\mathbf{x}} \\ \lambda \\ \kappa \\ \rho \end{pmatrix} \tag{28a}$$

and $b \in X^*$ is defined as

$$b = \begin{pmatrix} \delta_h\mathcal{E}_{\mathrm{tf}} \\ 0 \\ \delta_{\mathbf{x}}\mathcal{E}_{\mathrm{tf}} \\ 0 \\ 0 \\ 0 \end{pmatrix} = \begin{pmatrix} Sh + M\partial_h W \\ 0 \\ \nu M_\gamma(1 + \frac{1}{2}|\nabla h|^2) \\ 0 \\ 0 \\ 0 \end{pmatrix}. \tag{28b}$$

Note that M, D, S are defined in (24), whereas M_γ, C_γ, D_γ act as follows:

$$\left\langle \mathbf{v}, D_\gamma\,\mathbf{w}\right\rangle = \int_\gamma \mu_\gamma \mathbf{v}\cdot\mathbf{w}\,\mathrm{d}\gamma, \tag{29a}$$

$$\left\langle v, M_\gamma w\right\rangle = \int_\gamma v w\,\mathrm{d}\gamma, \tag{29b}$$

$$\langle v, C_\gamma \mathbf{w}\rangle = \int_\gamma v\,\mathbf{w}\cdot\nabla h\,\mathrm{d}\gamma, \tag{29c}$$

where $\mathbf{v}, \mathbf{w} : \gamma \to \mathbb{R}^{d-1}$, $v : \gamma \to \mathbb{R}$, and $w : \omega \to \mathbb{R}$. Additionally we defined $M_0\pi = \int_\omega \pi\,\mathrm{d}\mathbf{x}$. In the 6×6 block matrix A in (28a), the upper-left 3×3 block contains the dissipation, whereas the remaining parts contain the constraints. All the parts of A with a dot $(\cdot)$ are entirely zero. As before, from the block structure of A, we can reconstruct the PDE with the contact angle model, which we briefly outline. As before, we first eliminate the unknown Lagrange multiplier λ, κ, ρ. The first line of A gives $\lambda = \Delta h - \partial_h f$ and $\kappa = -\boldsymbol{\nu}\cdot\nabla h$. The third line then gives

$$\mu_\gamma\dot{\mathbf{x}} = -\kappa\nabla h - \boldsymbol{\nu}\left(1 + \frac{1}{2}|\nabla h|^2\right) = \boldsymbol{\nu}\left(\frac{1}{2}|\nabla h|^2 - 1\right),$$

where we used $\nabla h = -\boldsymbol{\nu}|\nabla h|$ and $\boldsymbol{\nu}\cdot\nabla h = -|\nabla h|$ to arrive at the contact angle model which we already observed directly in (19b). From the second line, we get $\rho = 0$ and $\pi = -\lambda$, and by inserting this into the constraint $\dot h - \nabla\cdot(m\nabla\pi) = 0$, we recover the thin-film model in (19). Including ρ removes a potential zero eigenvalue from the algebraic system. This identification confirms that the gradient structure in (28) corresponds to the thin-film model we obtained by the formal asymptotics.

D. Numerical implementation

The spatial discretization of the weak formulation in (28) is performed using standard P_1 finite elements. Since the resulting PDE will be of fourth-order parabolic type, an implicit time-discretization is advantageous to overcome the restrictions of the time-step size τ due to a Courant-Friedrichs-Lewy-type condition. A semi-implicit discretization can be achieved by replacing Sh in b with $S(h + \tau\dot h)$, which effectively modifies A such that we have the component $A_{\dot h\dot h} = \tau S$. A similar strategy might be useful for $\delta_{\mathbf{x}}\mathcal{E}_{\mathrm{tf}}$, but was not needed so far. Then $\dot h$ is computed by solving $Au = -b$. However, setting $h(t+\tau,\cdot) = h(t,\cdot) + \tau\dot h$ is ill-defined, since $h(t+\tau,\cdot)$ and $h(t,\cdot)$ are defined on different domains $\omega(t)$ and $\omega(t+\tau)$. However, using a diffeomorphism $\boldsymbol{\xi}(t,\cdot) : \omega(t_0) \to \omega(t)$ as we have defined it in Appendix B, we can pull-back $H(t,\mathbf{y}) = h(t,\boldsymbol{\xi}(t,\mathbf{y}))$ to the reference domain and recover time-derivatives $(\dot H, \dot{\boldsymbol{\xi}})$ in the *Arbitrary Lagrangian-Eulerian* (ALE) frame and update the corresponding discrete solution

$$H(t+\tau,\mathbf{y}) = H(t,\mathbf{y}) + \tau\dot H(\mathbf{y}), \tag{30a}$$

$$\boldsymbol{\xi}(t+\tau,\mathbf{y}) = \boldsymbol{\xi}(t,\mathbf{y}) + \tau\dot{\boldsymbol{\xi}}(\mathbf{y}), \tag{30b}$$

in the ALE reference frame. More details for the decomposition $\dot h \mapsto (\dot H, \dot{\boldsymbol{\xi}})$ and for the construction of mappings in higher spatial dimensions but without dynamic contact angle can be found in Ref. 27. The corresponding MATLAB code thin-film_clm.m written by the author is also available as a GitHub repository.[38]

IV. GRAVITY-DRIVEN DROPLETS

The flow of a viscous fluid on an incline is a subject that has been studied extensively in the past.[39–43] Research was devoted to understanding singularities and instability patterns of moving contact lines using different modeling approaches for the moving contact line. In the following, we solve the transient problem and show the impact contact angle models on sliding droplets for the thin-film free boundary problem with gravity and surface tension as driving forces. For given domain size L_0, we use initial data in the domain $\omega = (0, L_0)$ where $h_0(x) = \tan(\vartheta_e)\,x(L_0 - x)/L_0$, with equilibrium contact angle $\tan\vartheta_e = \sqrt{2}$ and volume $V = (\tan\vartheta_e)L_0^2/6$. In general, for a $3D$ droplet running down an incline plane, one would expect either of the two alternative scenarios:

(i) The solution becomes unstable and develops a topological transition. Due to a pinch-off singularity, the droplet decays into satellite droplets.[44] However, in one spatial dimension, pinch-off is not observed.

(ii) Instead, gravity-driven droplets approach traveling wave solutions H with constant velocity as $t \to \infty$, i.e.,

$$h(t,x) = H(\eta), \qquad \eta = (x - x_-) - Ut, \tag{31}$$

so that with $L = x_+ - x_-$ we have $\eta \in (0, L)$, $H : (0, L) \to \mathbb{R}$, and $\omega = (x_- + Ut, x_+ + Ut)$ for some $x_\pm, U \in \mathbb{R}$ and with contact line speed $\dot x_\pm = U$. At large volumes, these solutions become very elongated. Due to the specific form of the solution, one can

easily verify that with gravity as a driving force $W(h;x) = 4hx$ we have

$$\mathcal{E}_{\mathrm{tf}}(h(t,\cdot)) = \int_0^L 1 + \tfrac{1}{2}|H'|^2 + W(H;\hat{x}_- + Ut + \eta)\,\mathrm{d}\eta$$
$$= \mathcal{E}_{\mathrm{tf}}(\hat{h}(t=0,\cdot)) + 4Ut\int_0^L H\,\mathrm{d}\eta,$$

after transforming the original integral to a fixed domain. The time-derivative of the energy is $\dot{\mathcal{E}}_{\mathrm{tf}} = 4UV$. Rescaling $\pi = U\hat{\pi}$, we similarly get

$$\mathcal{D}_{\mathrm{tf}} = U^2\left(\int_0^L m(H)|\hat{\pi}'|^2\,\mathrm{d}\eta + 2\mu_\gamma\right),$$

where from (20) we get $(m(H)\hat{\pi}')' = -H'$ and used $\dot{h} = -UH'$. The balance $\dot{\mathcal{E}}_{\mathrm{tf}} = -\mathcal{D}_{\mathrm{tf}}$ implies a universal upper bound U_{lim} for the velocity (in 1D)

$$U = \frac{4V}{2\mu_\gamma + \int_0^L m(H)|\nabla\hat{\pi}|^2\,\mathrm{d}\eta} \le \frac{2V}{\mu_\gamma} = U_{\mathrm{lim}}, \qquad (32)$$

determined exclusively by the droplet volume V and the contact line dissipation μ_γ.

For the mobility $m(h) = h^2$ corresponding to a regime dominated by the Navier-slip boundary condition (14c), one has $\mathcal{D}_{\mathrm{tf}} = U^2(L + 2\mu_\gamma)$ (see Appendix D) so that we have an expression for the velocity where only $V(L)$ is unknown. For slowly moving small droplets, we will have $L \approx L_0$ and thereby $V(L) \approx \tan(\vartheta_e)L^2/6$ as $L \to 0$. Hence, for sufficiently small droplets and $m(h) = h^2$, we have the explicit expression for the velocity

$$U(L) = \tfrac{2}{3}\tfrac{L^2}{2\mu_\gamma + L}\tan\vartheta_e. \qquad (33)$$

These relations show that by systematically varying the droplet volume it is possible to probe different contributions to the droplet dissipation. In particular, for $L \to 0$ with the Navier-slip condition, the contact line dissipation will dominate and the limiting velocity U_{lim} is approached. However, for large volumes, these regimes might be practically irrelevant, since fluid flow for long times is dominated by other asymptotic regimes.[45]

In the following, we investigate the impact of different mobility laws $m(h)$ and different values for the contact line dissipation μ_γ on the long-time behavior of droplets. To show the general behavior, we solve the dynamic problem with $b = 1/6$, i.e., $m(h) = 2h^3 + h^2$. The traveling wave solutions $H(\eta)$ for different volumes are shown in Fig. 4. For smaller volumes, the solutions become more symmetrical and closer

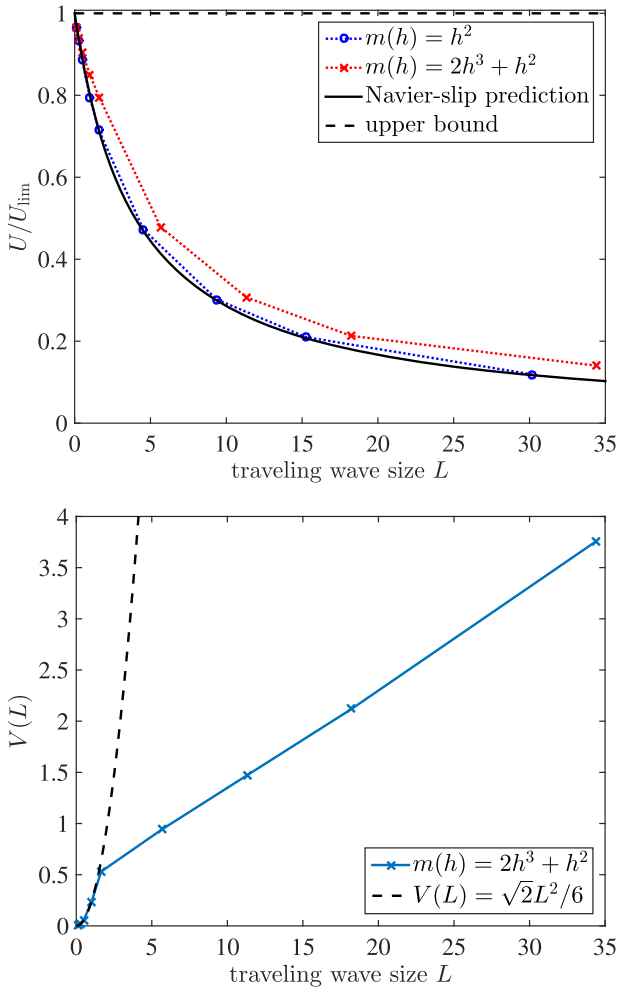

FIG. 5. (**Top**) Traveling wave solutions for different lengths L and different material parameters $m(h)$ give rise to different velocities $U \le U_{\mathrm{lim}}$ that are always bounded and $U \to U_{\mathrm{lim}}$ as $V, L \to 0$, see (32). (**Bottom**) For $m(h) = 2h^3 + h^2$, the relation of $V(L)$ shows symmetric droplets for $L < 2$ following $V \sim \sqrt{2}L^2/6$ and the nonsymmetric ones for $L > 2$.

to $H(\eta) = \tan\vartheta_e\eta(L - \eta)/L$. For sufficiently large volumes $V = \sqrt{2}L_0^2/6$, the symmetric droplets evolve into a strongly asymmetric shape, where a capillary ridge is connected to a region of nearly constant film thickness similar to a Landau-Levich film. Then, the support of the traveling wave solution L is considerably larger than the initial length L_0, as can be also seen in the bottom panel of Fig. 5. For larger droplet volumes, the shape of the capillary ridge does not change significantly and mostly the length of the zone of constant thickness does. The upper panel of Fig. 5 shows that the upper bound for

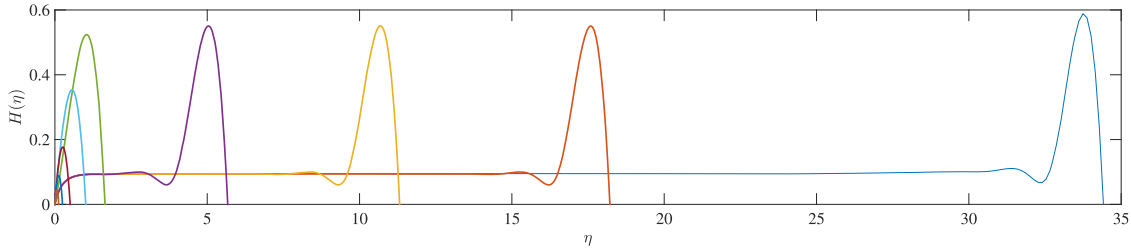

FIG. 4. Exemplary traveling wave solution $H(\eta)$ as in (31) with mobility law $m(h) = 2h^3 + h^2$, $\mu_\gamma = 2$ for different volumes $V = \sqrt{2}L_0^2/6$ where $L_0 \in$ (1/8, 1/4, 1/2, 1, 3/2, 2, 5/2, 3, 4) gives rise to different droplet velocities U.

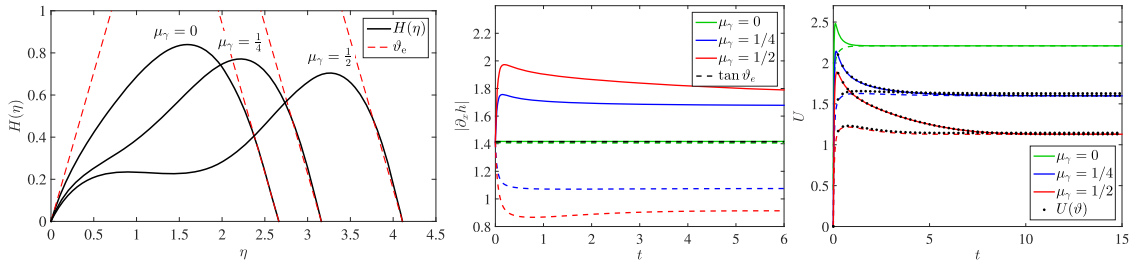

FIG. 6. Numerical solutions of the thin-film model with the contact angle model for $\mu_\gamma = 0$ (equilibrium) and $\mu_\gamma = 1/4$, $1/2$ (dynamic) showing (**left**) height in a comoving frame $H(\eta)$ with $\eta \in (0, L)$ computed from the solution of the full dynamic problem, (**middle**) contact angle *vs* time compared to equilibrium angle (black dashed), and (**right**) contact line velocity *vs* time compared to contact angle model (dots) for $V = 25\sqrt{2}/24$, $m(h) = h^2$ ($b \to \infty$). Slopes $|\partial_x h|$ and velocities U are evaluated at the advancing x_+ (solid) and receding x_- (dashed) side.

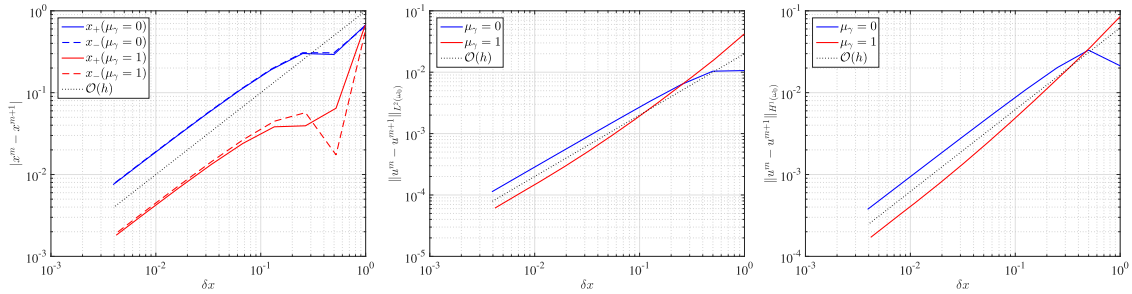

FIG. 7. Convergence of solutions at $T = 8$ for $\mu_\gamma = 0$ (blue) and $\mu_\gamma = 1$ (red) (**left**) for the positions of the contact points, (**middle**) for the L^2 norm of the solution, and (**right**) for the H^1 norm of the solution.

the velocity in (32) is generally valid and the Navier-slip prediction gives a good estimate even for the chosen mixed mobility with $b = 1/6$. Similar observations on symmetric and elongated solutions have been made, for instance, in the studies on stability analysis of sliding drops by Thiele *et al.*[42,46] In these studies, the contact line was regularized using a precursor potential, which then enters the stability considerations.

In Fig. 6, we discuss how the solutions of the dynamic system approach stationary shapes and how this is affected by different values of the contact line dissipation. For all solutions, the volume is fixed by setting $L_0 = 5/2$. The left panel of Fig. 6 shows the traveling wave solutions for $\mu_\gamma = 0$ (equilibrium angle) and for $\mu_\gamma = 1/4$, $1/2$ (dynamic contact angle). While for $\mu_\gamma = 0$ the solution is still rather symmetric, increasing the contact line dissipation to $\mu_\gamma = 1/2$ triggers the transition to elongated droplets at a smaller volume. Furthermore, only for $\mu_\gamma = 0$, the contact angle approaches the equilibrium value of $|\partial_x h| = \tan\vartheta_e = \sqrt{2}$ and the angle is smaller/larger at the receding/advancing side of the droplet for $\mu_\gamma > 0$. This is more evident in the middle panel of Fig. 6, where the time-evolution of the contact angle is shown. As the stationary shape is approached, the slopes at the advancing and receding side approach different constant values. For $\mu_\gamma = 0$ the contact slope has its equilibrium value $\sqrt{2}$ all the time with small differences due to some numerical dissipation. The right panel shows most clearly the convergence to the stationary shape, visible as the velocities at the advancing and receding side approach each other, i.e., compare full and dashed curves of same colors approaching each other for different μ_γ. With increasing contact line dissipation, the convergence to the stationary shape usually takes longer and the resulting velocity U is lower. The dots indicate the agreement with the velocity from the contact angle model (17).

In order to study the experimental rate of convergence as $\delta x \sim 2^{-m}\, L \to 0$ in space, we solve the problem on domains discretized using $2^m + 1$ points for $m = 1, \ldots, 10$ using $N_\tau = 25\,000$ uniform time steps and compare solutions at level m with solutions at neighboring levels $m + 1$. At the final time T, we compare solutions with respect to the convergence of $x_\pm(T)$ and use an affine map to pull back the solution $h(T, x)$ to a fixed domain $\omega_0 \approx \omega(T)$. On the fixed domain, we study the convergence of h with respect to the $L^2(\omega_0)$ and the $H^1(\omega_0)$ norm as $\delta x \sim 2^{-m}\, L \to 0$. The left panel of Fig. 7 shows the linear convergence of $|x_\pm^m - x_\pm^{m+1}|$ as $\delta x \to 0$ in both cases $\mu_\gamma = 0, 1$ with similar errors for x_- and x_+. However, note that the magnitude of the error appears slightly better for $\mu_\gamma = 1$. The middle and right panels of Fig. 7 show the convergence of the height profile $h(t, \xi(t, y))$ with $\xi(t, \cdot) : \omega_0 \to \omega(t)$ on a fixed domain ω_0, since solutions for different m are generally defined on different domains. Note that we have a linear rate of convergence in the $L^2(\omega_0)$ and also in the $H^1(\omega_0)$ norm.

V. CONCLUSION

This paper presented a gradient flow approach to dynamic contact angle models based on quadratic dissipation functionals. First a variational formulation is constructed for the Stokes flow and then reduced to a thin-film model. For the thin-film model, the variational form including constraints is stated explicitly and a time- and space-discretization is proposed. In one spatial dimension, a novel numerical scheme is constructed explicitly and used to study the motion of

gravity-driven on a vertical wall. These solutions confirm the general expectation of advancing and receding contact angles, where the asymmetry of moving droplets is strongly affected by the contact line dissipation and the droplet volume. We observe that the scheme leads to first order convergence of solutions in space and the method reproduces the predicted contact angle dynamics. Due to the inherent coupling of space and time in the free boundary problem, it is certainly a challenging task to construct higher order methods. It is expected that such a modification of the thin-film dynamics has a strong impact on pattern formation processes in higher dimensions, e.g., fingering of liquid sheet on an incline, dewetting of liquid films, and sliding of a $3D$ droplet on an incline. The corresponding extension of this method is therefore highly desirable.

ACKNOWLEDGMENTS

I am thankful for discussions with Luca Heltai (SISSA) and Marita Thomas (WIAS). This research is carried out in the framework of MATHEON supported by the Einstein Foundation Berlin.

APPENDIX A: HINTS CONCERNING THE NOTATION

The integration $\int \ldots \mathrm{d}\mathbf{x}\,\mathrm{d}z$, $\int \ldots \mathrm{d}\mathbf{x}$, $\int \ldots \mathrm{d}s$, and $\int \ldots \mathrm{d}\gamma$ refers to the d, $d-1$, and $d-2$ dimensional integration over Ω, ω, Γ, and γ, respectively. For $d=2$, the latter is the point evaluation at $(x_\pm, 0) \in \mathbb{R}^2$. The signed mean curvature is defined

$$\kappa = \frac{1}{d-1}\sum_{i=1}^{d-1} \kappa_i,$$

as the mean of the principle curvatures κ_i. The discretization of κ uses the identity $\kappa \boldsymbol{\nu}_\Omega = \underline{\Delta}\mathrm{id}_\Gamma$ for $\Gamma \subset \partial\Omega$, where details concerning the definition of the Laplace-Beltrami operator using the coordinate identity vector field $\mathrm{id}_\Gamma(\mathbf{x}, z) = (\mathbf{x}, z)$ can be found in Refs. 18 and 47.

APPENDIX B: ALE MAPPING OF $\dot{h}$

In two spatial dimensions, consider the reference interval at time t_0 given by $\omega_0 = (x_-^0, x_+^0)$ with $x_\pm^0 = x_\pm(t_0)$. For arbitrary time t, we define $\boldsymbol{\xi}(t,\cdot)\colon \omega_0 \to \omega(t)$ as

$$\boldsymbol{\xi}(t,y) = \Big(x_+(t) - x_-(t)\Big)\frac{y - x_-^0}{x_+^0 - x_-^0} + x_-(t)$$

so that $\boldsymbol{\xi}(t_0,\cdot) = \mathrm{id}_{\omega_0}$. Let $h(t,\cdot) : \omega(t) \to \mathbb{R}^+$ non-negative be defined on a time-dependent domain $\omega(t)$ with $h(t,\cdot) \equiv 0$ on the boundary $\partial\omega(t)$. The pull-back $H(t,\cdot) : \omega_0 \to \mathbb{R}^+$ of $h(t,\cdot)$ to the reference domain ω_0 is defined as

$$H(t,y) = h\big(t, \boldsymbol{\xi}(t,y)\big),$$

with the corresponding time-derivative

$$\dot{H}(t,y) = \dot{h}(t,\boldsymbol{\xi}) + \dot{\boldsymbol{\xi}}\cdot\nabla h(t,\boldsymbol{\xi}).$$

On $\partial\omega_0$, we have $\dot{H} \equiv 0$ and thereby $\dot{h} + \dot{\boldsymbol{\xi}}\cdot\nabla h = 0$ with $\dot{\boldsymbol{\xi}} = \dot{x}_\pm$. Since $\boldsymbol{\nu} = -\nabla h/|\nabla h|$ defines the outer normal, we can reconstruct the normal component of $\dot{\boldsymbol{\xi}}$ as

$$\dot{\boldsymbol{\xi}}\cdot\boldsymbol{\nu} = \frac{\dot{h}}{|\nabla h|}.$$

Except for the explicit form of $\boldsymbol{\xi}$ using $x_\pm$, all steps can be generalized to higher dimensions by solving an additional interpolation problem for $\boldsymbol{\xi}$.

APPENDIX C: UNCOMPENSATED YOUNG FORCE

The uncompensated Young force $\mathbf{f}_\gamma = (\sigma_\ell \boldsymbol{\nu}_{\Gamma_\ell} + \sigma_{s\ell}\boldsymbol{\nu}_{\Gamma_{s\ell}})$ in the contact angle model (14f) is multiplied with vectors $\mathbf{t}$ parallel to the $\mathbf{x}$-plane. When using $\mathbf{t} = \boldsymbol{\nu}_{\Gamma_\ell} = (\boldsymbol{\nu}, 0)$, with $\boldsymbol{\nu}$ the outer normal on $\partial\omega$, this produces

$$\mu_\gamma \boldsymbol{\nu}\cdot\mathbf{u}_\mathbf{x} = -\sigma_{s\ell} - \sigma_\ell\cos\vartheta, \tag{C1}$$

with surface tensions $\sigma_{s\ell} = \sigma_{\mathrm{solid,liquid}} - \sigma_{\mathrm{solid,air}}$ and $\sigma_\ell = \sigma_{\mathrm{liquid,air}}$. The equilibrium contact angle, when it can be defined, is $\sigma_{s\ell} = -\sigma_\ell\cos\vartheta_\mathrm{e}$ so that (C1) can be written as

$$\boldsymbol{\nu}\cdot\mathbf{u}_\mathbf{x} = \frac{\sigma_\ell}{\mu_\gamma}(\cos\vartheta_\mathrm{e} - \cos\vartheta). \tag{C2}$$

APPENDIX D: DISSIPATION OF TRAVELING WAVES WITH NAVIER-SLIP

A traveling wave solution with mobility $m(H) = H^2$ satisfies the elliptic equation

$$-H'(\eta) = (m(H)\hat{\pi}')',$$

in the bulk domain $\eta \in (0, L)$. In one spatial dimension using vanishing fluxes, this can be integrated $-H^{-1} = \hat{\pi}'$ so that the (bulk) dissipation becomes

$$U^{-2}\mathcal{D}_\mathrm{tf} = \int_0^L m(H)|\nabla\hat{\pi}|^2\,\mathrm{d}\eta = \int_0^L H^2(-1/H)^2\,\mathrm{d}\eta = L.$$

[1] P. G. De Gennes, "Wetting: Statics and dynamics," Rev. Mod. Phys. **57**(3), 827 (1985).
[2] A. Oron, S. H. Davis, and S. G. Bankoff, "Long-scale evolution of thin liquid films," Rev. Mod. Phys. **69**(3), 931 (1997).
[3] D. Bonn, J. Eggers, J. Indekeu, J. Meunier, and E. Rolley, "Wetting and spreading," Rev. Mod. Phys. **81**(2), 739 (2009).
[4] C. Huh and L. E. Scriven, "Hydrodynamic model of steady movement of a solid/liquid/fluid contact line," J. Colloid Interface Sci. **35**(1), 85–101 (1971).
[5] L. M. Hocking, "A moving fluid interface on a rough surface," J. Fluid Mech. **76**(4), 801–817 (1976).
[6] E. Lauga, M. Brenner, and H. Stone, "Microfluidics: The no-slip boundary condition," in *Springer Handbook of Experimental Fluid Mechanics* (Springer, 2007), pp. 1219–1240.
[7] A. Münch, B. A. Wagner, and T. P. Witelski, "Lubrication models with small to large slip lengths," J. Eng. Math. **53**(3-4), 359–383 (2005).
[8] A. B. D. Cassie and S. Baxter, "Wettability of porous surfaces," Trans. Faraday Soc. **40**, 546–551 (1944).
[9] E. B. Dussan, "On the spreading of liquids on solid surfaces: Static and dynamic contact lines," Annu. Rev. Fluid Mech. **11**(1), 371–400 (1979).
[10] Y. D. Shikhmurzaev, "The moving contact line on a smooth solid surface," Int. J. Multiphase Flow **19**(4), 589–610 (1993).
[11] T. Qian, X. P. Wang, and P. Sheng, "A variational approach to moving contact line hydrodynamics," J. Fluid Mech. **564**, 333–360 (2006).
[12] W. Ren and W. E, "Boundary conditions for the moving contact line problem," Phys. Fluids **19**(2), 022101 (2007).
[13] J. H. Snoeijer and B. Andreotti, "Moving contact lines: Scales, regimes, and dynamical transitions," Annu. Rev. Fluid Mech. **45**, 269–292 (2013).

[14]R. G. Cox, "The dynamics of the spreading of liquids on a solid surface. Part 1. Viscous flow," J. Fluid Mech. **168**, 169–194 (1986).
[15]O. V. Voinov, "Hydrodynamics of wetting," Fluid Dyn. **11**(5), 714–721 (1976).
[16]M. J. De Ruijter, T. D. Blake, and J. De Coninck, "Dynamic wetting studied by molecular modeling simulations of droplet spreading," Langmuir **15**(22), 7836–7847 (1999).
[17]T. D. Blake, "The physics of moving wetting lines," J. Colloid Interface Sci. **299**(1), 1–13 (2006).
[18]E. Bänsch, "Finite element discretization of the Navier-Stokes equations with a free capillary surface," Numerische Math. **88**(2), 203–235 (2001).
[19]Y. Sui, H. Ding, and P. D. M. Spelt, "Numerical simulations of flows with moving contact lines," Annu. Rev. Fluid Mech. **46**, 97–119 (2014).
[20]F. Montefuscolo, F. S. Sousa, and G. C. Buscaglia, "High-order ALE schemes for incompressible capillary flows," J. Comput. Phys. **278**, 133–147 (2014).
[21]J. C. Flitton and J. R. King, "Moving-boundary and fixed-domain problems for a sixth-order thin-film equation," Eur. J. Appl. Math. **15**(6), 713–754 (2004).
[22]F. B. Belgacem, M. V. Gnann, and C. Kuehn, "A dynamical systems approach for the contact-line singularity in thin-film flows," Nonlinear Anal. **144**, 204–235 (2016).
[23]L. Zhornitskaya and A. L. Bertozzi, "Positivity-preserving numerical schemes for lubrication-type equations," SIAM J. Numer. Anal. **37**(2), 523–555 (1999).
[24]G. Grün and M. Rumpf, "Nonnegativity preserving convergent schemes for the thin film equation," Numerische Math. **87**(1), 113–152 (2000).
[25]M. Bertsch, L. Giacomelli, and G. Karali, "Thin-film equations with partial wetting energy: Existence of weak solutions," Phys. D **209**(1-4), 17–27 (2005).
[26]H. Knüpfer, "Well-posedness for the Navier slip thin-film equation in the case of partial wetting," Commun. Pure Appl. Math. **64**(9), 1263–1296 (2011).
[27]D. Peschka, "Thin-film free boundary problems for partial wetting," J. Comput. Phys. **295**, 770–778 (2015).
[28]R. Huth, S. Jachalski, G. Kitavtsev, and D. Peschka, "Gradient flow perspective on thin-film bilayer flows," J. Eng. Math. **94**, 43–61 (2014).
[29]K. B. Glasner and T. P. Witelski, "Coarsening dynamics of dewetting films," Phys. Rev. E **67**(1), 016302 (2003).
[30]L. Giacomelli and F. Otto, "Rigorous lubrication approximation," Interfaces Free Boundaries **5**(4), 483–529 (2003).
[31]U. Thiele, D. V. Todorova, and H. Lopez, "Gradient dynamics description for films of mixtures and suspensions: Dewetting triggered by coupled film height and concentration fluctuations," Phys. Rev. Lett. **111**(11), 117801 (2013).
[32]X. Xu, U. Thiele, and T. Qian, "A variational approach to thin film hydrodynamics of binary mixtures," J. Phys.: Condens. Matter **27**(8), 085005 (2015).
[33]H. von Helmholtz, "Zur Theorie der stationären Ströme in reibenden Flüssigkeiten," Verh. Naturh.-Med. Ver. Heidelb. **11**, 223–230 (1868).
[34]M. A. Peletier, "Variational modelling: Energies, gradient flows, and large deviations," preprint arXiv:1402.1990 (2014).
[35]P. J. Morrison, "Hamiltonian description of the ideal fluid," Rev. Mod. Phys. **70**(2), 467 (1998).
[36]M. H. Giga, A. Kirshtein, and C. Liu, "Variational modeling and complex fluids," in *Handbook of Mathematical Analysis in Mechanics of Viscous Fluids* (Springer, Cham, 2017), pp. 1–41.
[37]J. T. Beale, "The initial value problem for the Navier-Stokes equations with a free surface," Commun. Pure Appl. Math. **34**(3), 359–392 (1981).
[38]D. Peschka, A MATLAB algorithm for thin-film free boundary problems in one spatial dimension, https://github.com/dpeschka/thinfilm-freeboundary, 2017.
[39]L. M. Hocking, "Sliding and spreading of thin two-dimensional drops," Q. J. Mech. Appl. Math. **34**(1), 37–55 (1981).
[40]L. M. Hocking and M. J. Miksis, "Stability of a ridge of fluid," J. Fluid Mech. **247**, 157–177 (1993).
[41]L. Kondic and J. Diez, "Pattern formation in the flow of thin films down an incline: Constant flux configuration," Phys. Fluids **13**(11), 3168–3184 (2001).
[42]U. Thiele, K. Neuffer, M. Bestehorn, Y. Pomeau, and M. G. Velarde, "Sliding drops on an inclined plane," Colloids Surf., A **206**(1-3), 87–104 (2002).
[43]N. Savva and S. Kalliadasis, "Droplet motion on inclined heterogeneous substrates," J. Fluid Mech. **725**, 462–491 (2013).
[44]J. H. Snoeijer, N. Le Grand-Piteira, L. Limat, H. A. Stone, and J. Eggers, "Cornered drops and rivulets," Phys. Fluids **19**(4), 042104 (2007).
[45]H. E. Huppert, "Flow and instability of a viscous current down a slope," Nature **300**(5891), 427 (1982).
[46]U. Thiele and E. Knobloch, "Front and back instability of a liquid film on a slightly inclined plate," Phys. Fluids **15**(4), 892–907 (2003).
[47]G. Dziuk, "An algorithm for evolutionary surfaces," Numerische Math. **58**(1), 603–611 (1990).